






Article

A Miniaturized Triple-Band Antenna Based on Square Split Ring for IoT Applications

Duaa H. Abdulzahra ¹, Falih Alnahwi ¹, Abdulkareem S. Abdullah ¹, Yasir I. A. Al-Yasir ^{2,*}
and Raed A. Abd-Alhameed ^{2,3}

¹ Department of Electrical Engineering, College of Engineering, University of Basrah, Basrah 61001, Iraq

² Faculty of Engineering and Informatics, University of Bradford, Bradford BD7 1DP, UK

³ Department of Information and Communication Engineering, Basrah University College of Science and Technology, Basra 61004, Iraq

* Correspondence: y.i.a.al-yasir@bradford.ac.uk; Tel.: +44-127-423-8047

Abstract: This article presents a miniaturized triple-band antenna for Internet of Things (IoT) applications. The miniaturization is achieved by using a split square ring resonator and half ring resonator. The antenna is fabricated on an FR4 substrate with dimensions of $(33 \times 22 \times 1.6)$ mm³. The proposed antenna resonates at the frequencies 2.4 GHz, 3.7 GHz, and 5.8 GHz for WLAN and WiMax applications. The obtained -10 dB bandwidth for the three bands of the proposed antenna are 300 MHz, 360 MHz, and 900 MHz, respectively. The measured reflection coefficient values of the proposed antenna corresponding to each resonant frequency are equal to -14.772 dB, -20.971 dB, and -28.1755 dB, respectively. The measured gain values are 1.43 dBi, 0.89 dBi, and 1 dBi, respectively, at each resonant frequency. There is a good agreement between the measured and simulated results, and both show an omnidirectional radiation pattern at each of the antenna resonant frequencies that is suitable for IoT portable devices.



Citation: Abdulzahra, D.H.; Alnahwi, F.; Abdullah, A.S.; Al-Yasir, Y.I.A.; Abd-Alhameed, R.A. A Miniaturized Triple-Band Antenna Based on Square Split Ring for IoT Applications. *Electronics* **2022**, *11*, 2818. <https://doi.org/10.3390/electronics11182818>

Academic Editor: Reza K. Amineh

Received: 2 August 2022

Accepted: 5 September 2022

Published: 7 September 2022

Publisher's Note: MDPI stays neutral with regard to jurisdictional claims in published maps and institutional affiliations.



Copyright: © 2022 by the authors. Licensee MDPI, Basel, Switzerland. This article is an open access article distributed under the terms and conditions of the Creative Commons Attribution (CC BY) license (<https://creativecommons.org/licenses/by/4.0/>).

Keywords: multiband antenna; IoT applications; reflection coefficient; monopole; split ring resonator (SRR)

1. Introduction

Internet of things (IoT) represents a brand of communication technology that incorporates different wireless communication systems, like Wireless Local Area Network (WLAN), Wireless Sensor Networks (WSNs), Global System for Mobile Communication (GSM), Long Term Evolution (LTE), and so on. The rapid development of IoT leads to increase the challenges of designing multiband antenna with compact size and broad bandwidth to be integrated with IoT devices [1]. Expanding wireless technologies and services need compact antenna designs operating for wideband applications. Therefore, many researches are motivated to propose multiple band antennas with a compact antenna size.

The interconnection of devices like cellphones, sensors, computers and tablets, etc. can be achieved by IoT technology for collecting data around the world and sharing them through the internet to be utilized for various purposes. Many fields can be connected with IoT such as smart homes, smart cities, smart transportation, smart agriculture, smart health systems, as well as the WLAN applications [2,3]. These applications require components with a low profile, lightweight, and low cost to be integrated within the devices. Printed antenna is preferred to satisfy these requirements because of its special characteristics [4].

There are three types of antennas that are mainly used in recent years to investigate most of the above-mentioned bands, namely, planar monopole antennas [5], microstrip antennas [6], and slot antennas [7]. All of these types require a compact size and simple design. In studies [8,9], monopole antennas were presented for mobile phone integration because they have good radiation properties and planar structure which make them easy to be fabricated and integrated within the systems. In study [10], a monopole antenna

was designed depending on inserting different resonators for a multiband with a whole size of $(35 \times 32 \times 1.6) \text{ mm}^3$, while it has less than 0 dBi gain for each of 2.4 GHz and 5.8 GHz bands. A slot antenna was presented for multiple resonant frequencies which has the overall dimensions of $(70 \times 70 \times 2) \text{ mm}^3$ for wearable applications [7].

The conventional way to satisfy multiband properties for these antennas is either by etching slots or (or slits) in the radiator element [7,11], or by adding stubs to the radiator element. These techniques are used to perform different paths of the surface current that cause multiple resonant frequencies. Many methods were proposed for introducing antennas with compact size such as presenting a split ring resonator (SRR) by producing a negative- μ [12], using high permittivity material [13], and inserting slots that cause some changes in the current path to produce smaller physical length compared to the electrical length [14]. A defected ground plane is also one of the techniques that provides small size antenna such as in [15] where the ground plane was engraved by U-shaped slots. There are also different techniques that were previously introduced to satisfy multiband antenna design [16–19].

A compact planar MIMO antenna in [16] was operated for different wireless communication bands, which are preferable in the IoT applications. The designed antenna has overall dimensions of $(120 \times 65 \times 1.56) \text{ mm}^3$ which was used for handheld devices. In study [17], a reconfigurable antenna of $(80 \times 80 \times 1.6) \text{ mm}^3$ was presented by using six pin diodes to surpass the conventional antennas that serve a single frequency at a time. In study [18], an octahedron CPW antenna was proposed to be integrated with IoT devices. The antenna has a multiband response with dimensions of $(130 \times 90 \times 6.35) \text{ mm}^3$. In study [19], a monopole printed antenna was introduced to cover GSM, WLAN, and WiMAX bands for laptop devices with overall dimensions of $(200 \times 260 \times 1.6) \text{ mm}^3$, and it has a nearly omnidirectional radiation pattern with maximum gain of 4 dBi. Many designers and researchers used SRR for satisfying small size antennas. In study [20], the researchers used two of the SRRs with different sizes to get dual bands resonating at 4.72 GHz with an efficiency of 15%, 5.76 GHz with efficiency of 40%, and 5.76 GHz with efficiency of 40%. In study [21], complementary split ring resonator (CSRR) was used to decrease the physical size of the patch antenna. In study [22], an SRR and a closed ring resonator were combined to produce multiband antenna with small size. In study [23], a dual port antenna with slotted patch element was designed for IoT sensors at resonant frequencies of 1.73 and 2.4 GHz. The maximum realized gains are -3.8 dBi and 1.9 dBi with an overall size of $48 \text{ mm} \times 48 \text{ mm}$. In study [24], a quad band MIMO antenna was presented for IoT applications. It covered (GSM, WLAN, WiMAX, and 5G) bands with a size of $(60 \times 60 \times 1.6) \text{ mm}^3$. In study [25], a dual-band antenna was presented for IoT applications with a slotted square patch. It has a compact size of $(38.5 \times 38.5 \times 1.6) \text{ mm}^3$ and bandwidth of 20 MHz for each resonant mode. The design was tested with FR-4 substrate, whereas the realized gain values were less than 0 dBi. Therefore, they suggested using a Rogers Duroid 5880 substrate to enhance the gain, and then the simulated results showed 3.4 dBi and 3.2 dBi for 2.4 GHz and 2.8 GHz, respectively.

In this article, a compact triple-band antenna for IoT applications is proposed. The antenna radiating patch is a combination of a split square ring resonator shape and half ring resonator shape that results in a compact size of $(33 \times 22 \times 1.6) \text{ mm}^3$ with multiple resonance behavior. The proposed antenna is fabricated on a low-cost FR4 substrate, and it resonates at frequencies 2.4 GHz, 3.7 GHz, and 5.8 GHz for WLAN and WiMax applications.

In Section 2, the design steps of the proposed triple-band antenna based on SRR are presented. A parametric study has been conducted in Section 3 on the most effective parameters on the operation of the proposed design in order to obtain their optimized values. In Section 4, the simulated and measured results of the proposed antenna are presented along with a comparison with some relevant works. The main conclusions of this work are summarized in Section 5.

2. Antenna Design

The proposed antenna configuration is shown in Figure 1. The initial design is based on the conventional rectangle monopole antenna shown in Figure 2a using a low-cost FR4 substrate that has a dielectric constant of 4.3, loss tangent of 0.025, and height of 1.6 mm. The FR-4 substrate is solid and not flexible, which is needed in the design. In addition, it has a higher value of ϵ_r that leads to a more compact size and wider bandwidth. In addition, this type of substrate is considered as a low-cost material compared with other types of substrates but still, there is some dissipation that appears at higher frequencies which make an effect on the bandwidth. The radiating element of the antenna is at the top side of the substrate, and a partial ground plane is at its rear side. A microstrip feed line of 50Ω characteristic impedance is used to ensure a good impedance matching. The performance of the design is assumed according to the following metrics: the three bands of the proposed antenna should have reflection coefficient values less than -10 dB, gain values above 0 dBi, and radiation efficiency values above 50% with omnidirectional patterns that ensure a good coverage for IoT portable applications. Moreover, the bandwidth for each band is considered with a threshold reflection coefficient value of -10 dB. The overall size of the proposed antenna is $33 \text{ mm} \times 22 \text{ mm}$, and the initial values of the parameters are given in Table 1. The reflection coefficient response of the initial design is shown in Figure 2b. The conventional design equations in [26] are used for the initial microstrip antenna at a center frequency of 3 GHz. The antenna length is then reduced to $\lambda_g/4$ because the microstrip antenna is converted to a planar monopole antenna by the partial coverage of the ground plane [26].

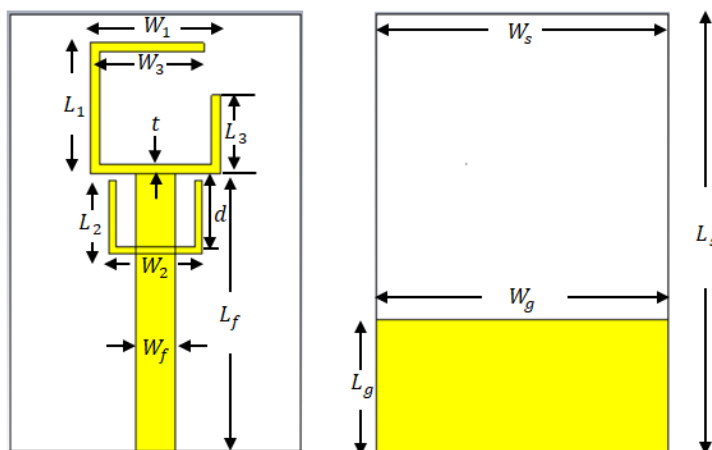


Figure 1. The proposed antenna structure.

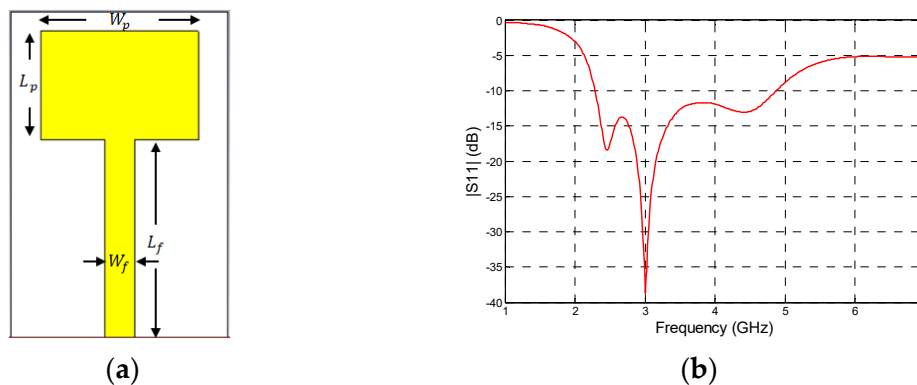


Figure 2. (a) The conventional rectangular shape and (b) Its simulated reflection coefficient response.

Table 1. The initial dimensions of the proposed antenna.

Parameter	Dimension (mm)	Parameter	Dimension (mm)
W_s	22	W_p	16
L_s	33	L_p	11
L_g	14	L_f	20
W_g	22	W_f	3

These conventional equations give an initial knowledge of the radiating element dimensions, which are modified to reduce the frequency while keeping the compact size. In addition, they are presented to produce dual band, and the evolution process is done by using different techniques such as cutting slots in the radiating element that performs a new shape with different response. Moreover, using meander line is considered one of the methods to satisfy a small-size antenna so that the proposed antenna starting with conventional design shape with a frequency located in the middle of the desired three bands to gain more reduction in the antenna size because increasing the value of the frequency results in smaller antenna size. Secondly, in Figure 3a, the designed parameters are optimized, and also the radiator shape is changed to a square ring resonator of 0.71 mm thickness, which leads to two resonant frequencies at 2.37 GHz and 6.8 GHz with corresponding reflection coefficients of -21.851 dB and -39.97 dB as declared in Figure 3b. Thirdly, the square ring is cut from the upper right corner to produce a split ring resonator (SRR) which leads to a shift in the second frequency to 3.7 GHz with a reflection coefficient of -28.301 dB as shown in Figure 4a,b.

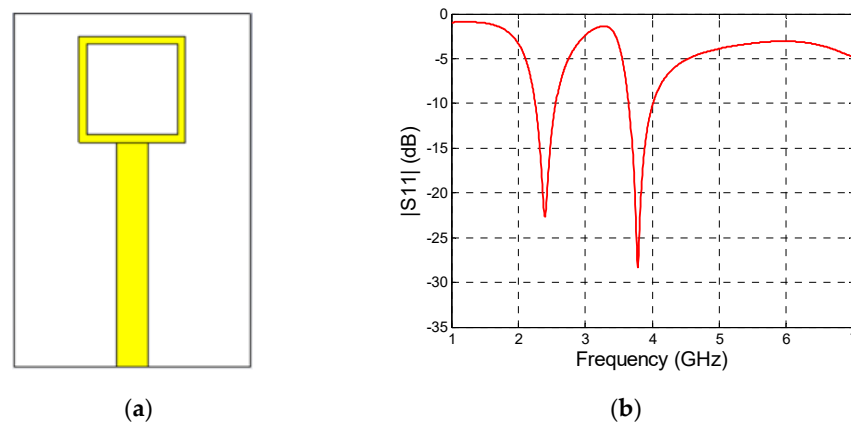


Figure 3. (a) The square ring radiator element and (b) Its simulated reflection coefficient response.

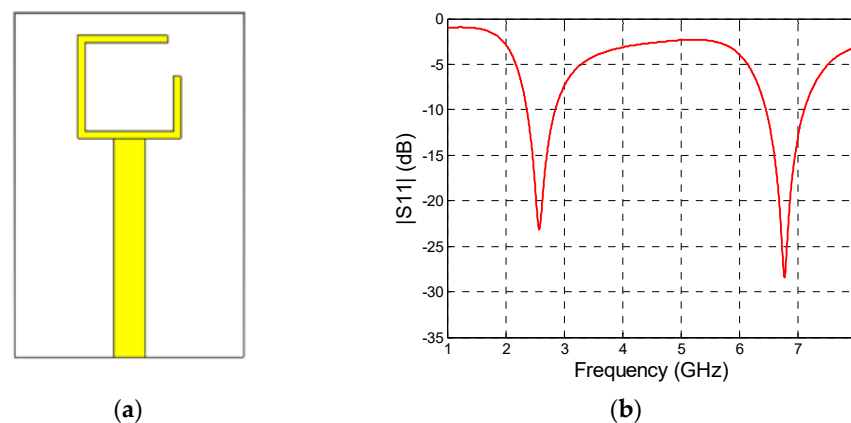


Figure 4. (a) The split ring resonator and (b) Its simulated reflection coefficient response.

The usual way to resonate multiple frequencies that are adopted in this work is by adding parasitic elements. Finally, to generate the third band, another half ring of 0.53 mm thickness and 5.5 mm away from the first ring is added. This element ensures the appearance of the third resonant frequency at 5.8 GHz with -29.616 dB reflection coefficient as shown in Figure 5a,b. It is clear from the design steps that the surface current distribution is changed on each step so that it causes the generation of additional resonant frequencies. The equivalent circuit of the antenna according to [27] is shown in Figure 6 where R1, L1, and C1 represent the parameters that generates the first resonance frequency 2.4 GHz. R2, L2, and C2 are for the generation of the second resonance frequency 3.7 GHz. Finally R3, L3, and C3 represent the elements that are responsible for the generation of the third resonance frequency 5.8 GHz. These parameters are calculated by using the following equations with respect to the three resonant frequencies [28].

$$\omega_r = 2\pi f_o \tag{1}$$

$$f_o = \frac{1}{2\pi\sqrt{LC}} \tag{2}$$

$$Q = \frac{f_o}{BW} = \frac{\omega_r L}{R} \tag{3}$$

$$C = \frac{\epsilon_o \epsilon_r S}{h} \tag{4}$$

where, ω_r represents the angular frequency in (rad/sec.), f_o is the resonant frequency in GHz, L denotes the inductance, C is the capacitance, R represents the resistance, Q is the quality factor, BW is the bandwidth, ϵ_o denotes the permittivity of free-space, ϵ_r is the dielectric constant, and h represents the substrate height. In addition, S represents the surface area of the antenna parts that radiate each band. Table 2 lists the calculated parameters of the equivalent circuit corresponding to each resonant frequency. NI Multisim version 11 is used to draw the circuit diagram.

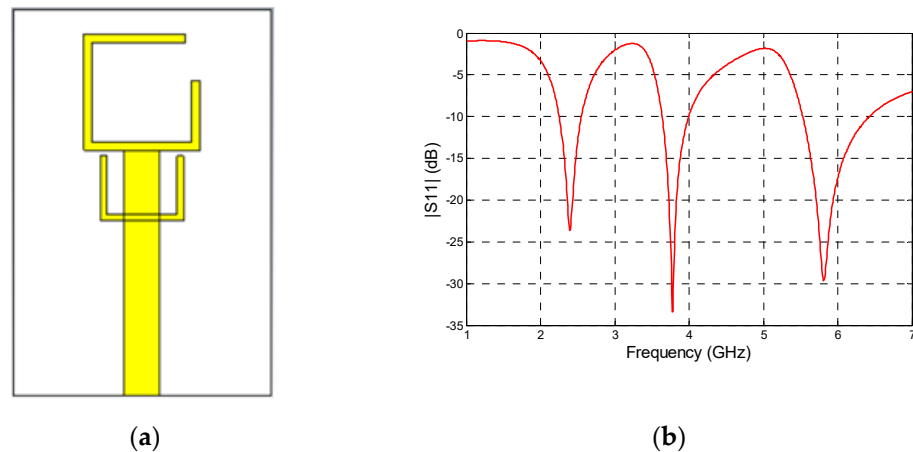


Figure 5. (a) The addition of the second half ring and (b) Its simulated reflection coefficient response.

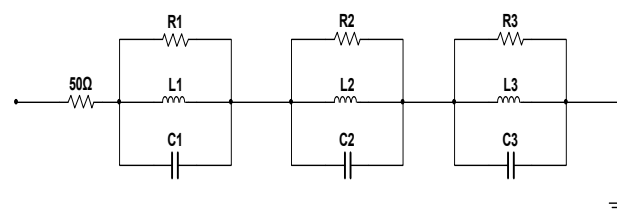


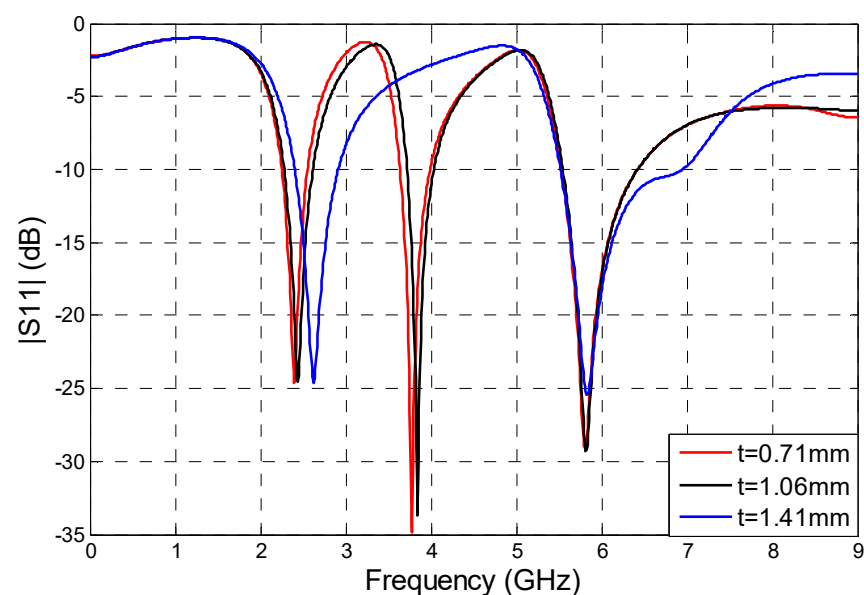
Figure 6. The equivalent circuit of the proposed antenna.

Table 2. The parameters of RLC equivalent circuit of the proposed antenna.

Parameters	Values	Parameters	Values	Parameters	Values
R_1	50.2 Ω	R_2	49 Ω	R_3	47 Ω
L_1	26.67 nH	L_2	19.87 nH	L_3	8.219 nH
C_1	0.1649 pF	C_2	0.09311 pF	C_3	0.091 pF

3. Parametric Study

For choosing the proper structure of the antenna, the initial design was changed over the development steps process as detailed earlier in Section 2. In this article, a partial ground plane was used for achieving good radiation characteristics and the radiating element consists of a full and half square rings shape that are introduced after starting with the conventional square-shaped patch antenna. Thence, a slot is engraved to get a square ring shape that produces two different bands, and then the ring is converted to a split ring. Finally, a second half ring resonator is adding to produce an antenna with triple-band. Different parameters are optimized according to the parametric analysis to obtain the modified parameters. The most effective parameters on the operation of the proposed design are the width of the SRR and the distance between the two rings. When all parameters are kept constant and varying the width of the split ring resonator (t), Figure 7 shows the effect of this parameter on the first and second resonance frequencies. Both frequencies are shifted to higher values at $t = 1.06$ mm and at $t = 1.41$ mm with a little reduction in the reflection coefficient value. Furthermore, at $t = 1.41$ mm, the second frequency is completely eliminated. Therefore, $t = 0.71$ mm is selected since it gives the first resonant frequency at the 2.4 GHz WLAN and the second at 3.7 GHz WiMax applications with minimum reflection coefficient values. The second parameter that affects the response of the reflection coefficient is the distance (d) between the bottom end of the split square ring and the other half ring. This distance affects the location of the third resonant frequency, and it is found that it is located at 5.8 GHz at $d = 5.5$ mm. However, it is shifted to more than 6 GHz in the other two distance values with a reduction in the return loss performance as shown in Figure 8. According to the parametric study, the final structure of the proposed antenna is optimized as listed in Table 3. All the simulation results are obtained with the aid of CST Microwave Studio software [27].

**Figure 7.** The effect of SRR width on the reflection coefficient of the proposed antenna.

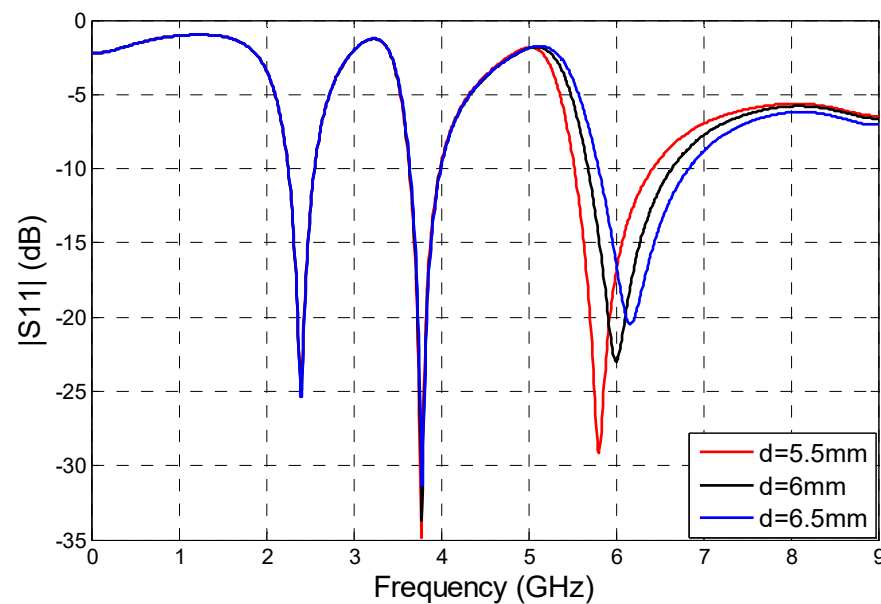


Figure 8. The effect of the distance between the two rings on the reflection coefficient of the proposed antenna.

Table 3. The optimized parameters of the proposed antenna.

Parameter	Dimension (mm)	Parameter	Dimension (mm)
W_s	22	L_1	9.9
L_s	33	W_1	9.9
L_g	10	L_2	5.54
W_g	22	W_2	7.07
L_f	21	L_3	5.95
W_f	3	W_3	8.63
D	5.5	T	0.71

4. Results

The front and rear views of the fabricated antenna are shown in Figure 9. The measurements were acquired using Amitec transceiver with a directional coupler, and Figure 10a demonstrates the setup of measuring the reflection coefficient of the proposed multiband antenna, while Figure 10b shows the measurement setup of the suggested antenna inside an anechoic chamber for measuring the gain and radiation pattern. Figure 11 illustrates the simulated and measured reflection coefficients of the three bands for the final antenna design. The simulated reflection coefficient values at each of the three resonance frequencies (2.4 GHz, 3.7 GHz, and 5.8 GHz) are pointed as -23.57 dB, 33.34 dB, and -29.62 dB, whereas the measured values of each band are -14.772 dB, -20.971 dB, -28.1755 dB at 2.55 GHz, 3.95 GHz, 6 GHz, respectively. The simulated bandwidth covers the range from 2.25 GHz to 2.55 GHz with a 12.5% fractional bandwidth for the first resonant frequency, from 3.6 GHz to 3.99 GHz with a 9.7% fractional bandwidth for the second resonant frequency, and from 5.5 GHz to 6.4 GHz with 15.5% fractional bandwidth for the third resonant frequency. On the other hand, the measured bandwidth extends along the range from 2.5 GHz to 2.7 GHz with a 7.8% fractional bandwidth for the first resonant frequency and from 3.8 GHz to 4.2 GHz with 10.1% fractional bandwidth for the second resonant frequency and from 5.65 GHz to 6.55 GHz with 15% fractional bandwidth for the third resonant frequency. The machine that is used to engrave the antenna is LPKF ProtoMat S42 laser cutting CNC machine. The deviations between the measured and simulated values of

the reflection coefficient are due to the fabrication imperfections of the CNC machine and the imperfect soldering of the SMA connector. Figure 12 displays the simulated surface current distributions of the proposed antenna at 2.4 GHz, 3.7 GHz, and 5.8 GHz. From Figure 12a, it is clear that the maximum current is concentrated at the left edge of the ring resonator, while the majority of the current is concentrated at the right edge of the ring resonator as shown in Figure 12b. The third band is introduced by inserting another half ring at a specific distance from the split ring so that Figure 12c clearly shows the concentration of the current at the half ring.

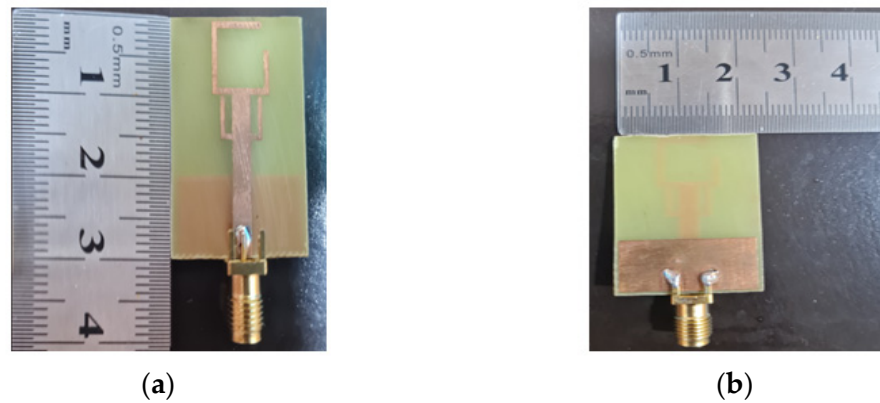


Figure 9. The fabricated antenna (a) front view (b) back view.



Figure 10. The measurement setup of (a) the reflection coefficient curve and (b) the radiation pattern and gain.

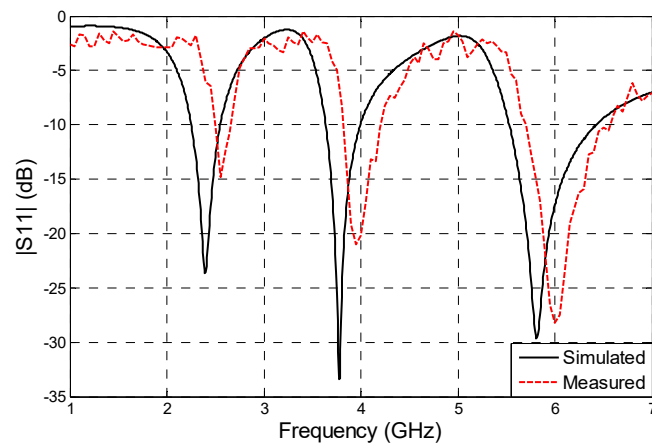


Figure 11. The simulated and measured reflection coefficients of the proposed antenna.

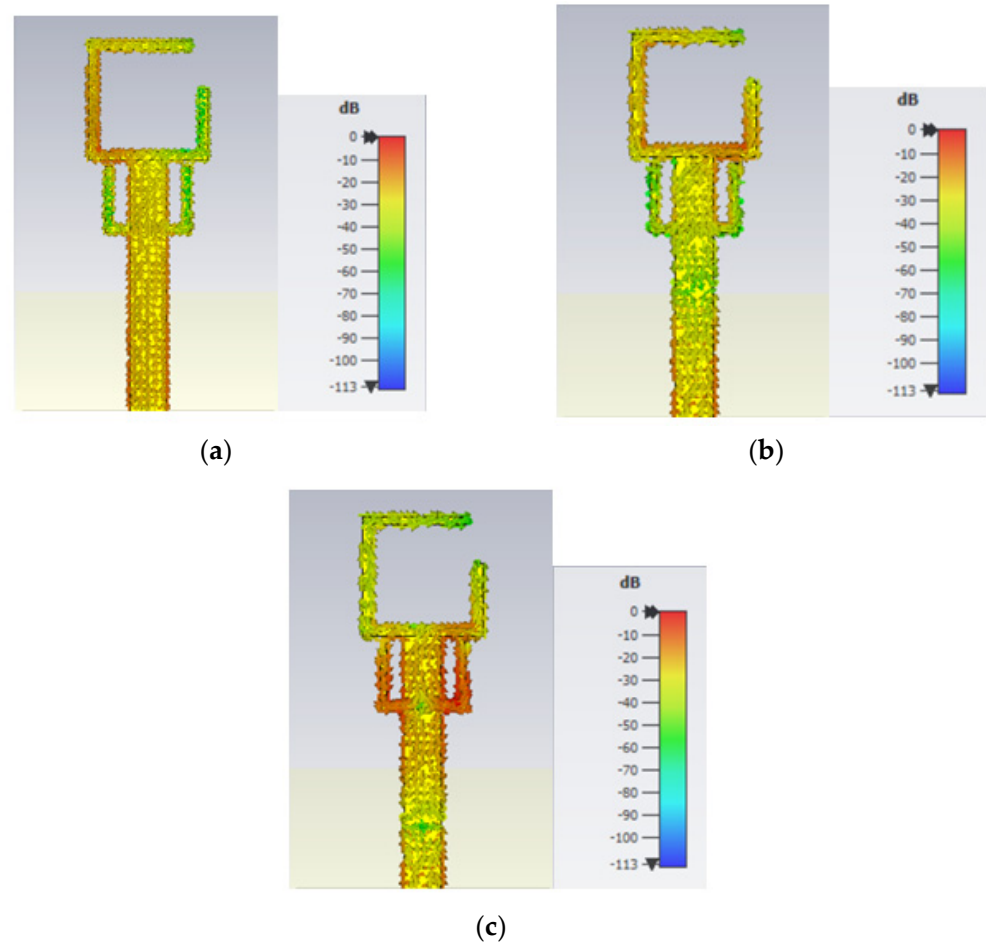


Figure 12. The simulated current distribution of the proposed design at (a) 2.4 GHz, (b) 3.7 GHz, and (c) 5.8 GHz.

The simulated and measured normalized power patterns of the final structure at the three resonant frequencies are shown in Figure 13. The E-plane and H-plane patterns are bidirectional and omnidirectional, respectively, for all of the three bands, which is almost preferable for the IoT portable devices. According to these patterns, the radiation for each frequency is independent of the orientation of the IoT devices so that it facilitates the connection of the antenna with the other IoT devices. Figure 14 shows the variation of the simulated and measured gain values as a function of frequency for the three bands (2.25–2.55) GHz, (3.6–3.99) GHz, and (5.5–6.4) GHz. The maximum simulated and measured gain values are found to be equal to 1.6 dBi and 1.43 dBi, for 2.4 GHz and 2.55 GHz, respectively. The other two bands have maximum measured gain values of 0.9 dBi and 1.1 dBi. Furthermore, the simulated values of the radiation efficiency at each frequency band are 82.5%, 72%, and 68%, respectively, while the measured values are 80.02%, 69.89%, and 67.1%, respectively. Figure 15 illustrates the radiation efficiency as a function of the frequency for the proposed antenna. There is some deviation between the measured and simulated results that are due to many issues such as the imperfect engraving of the CNC machine, the inaccurate soldering of the SMA connector, irregular variation of the dielectric constant of the substrate along the frequency, and the reflections of the surrounding objects inside the anechoic chamber.

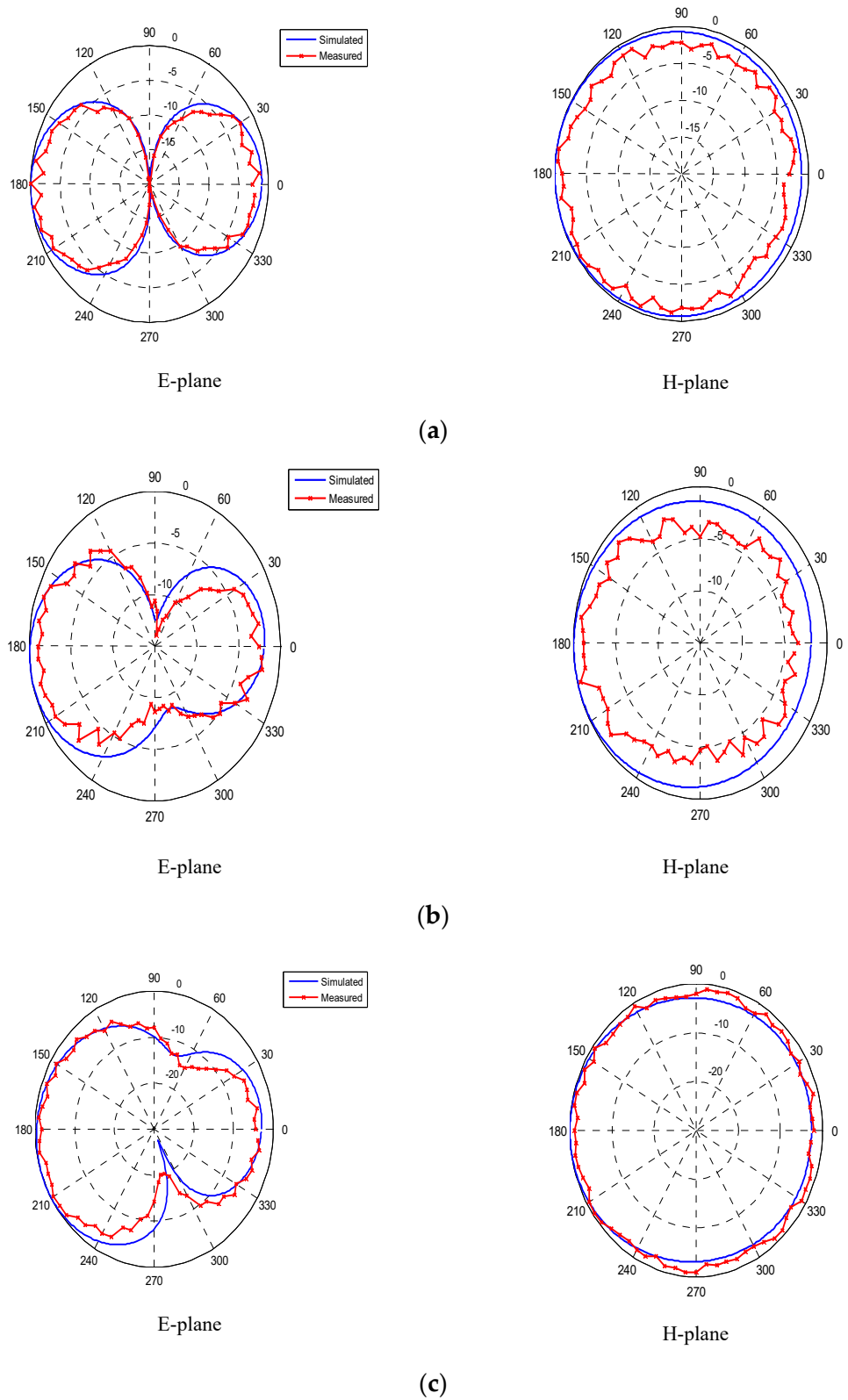


Figure 13. Radiation patterns of the proposed design at (a) 2.4 GHz, (b) 3.7 GHz, and (c) 5.8 GHz.

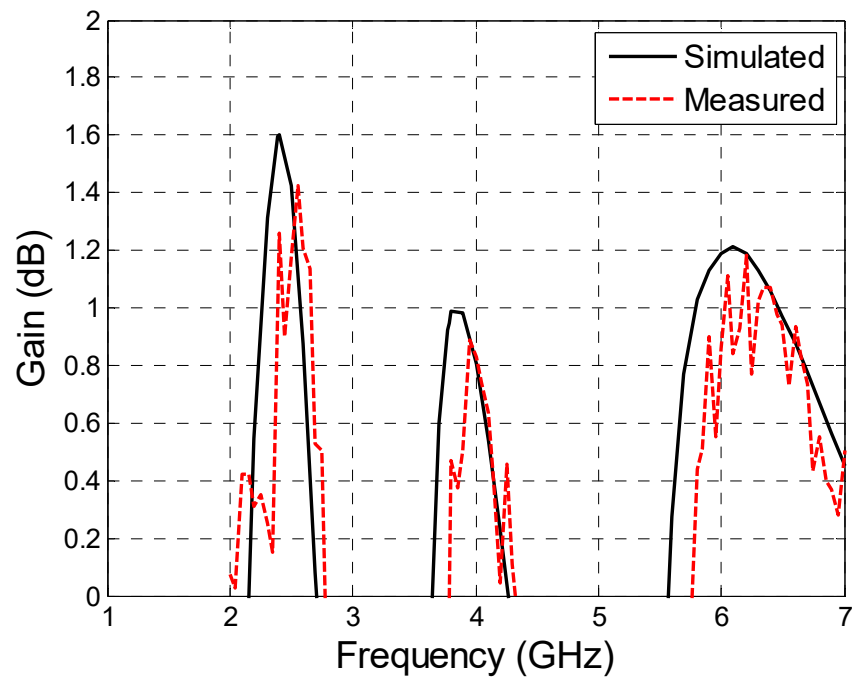


Figure 14. Variation of the proposed antenna gain as a function of frequency.

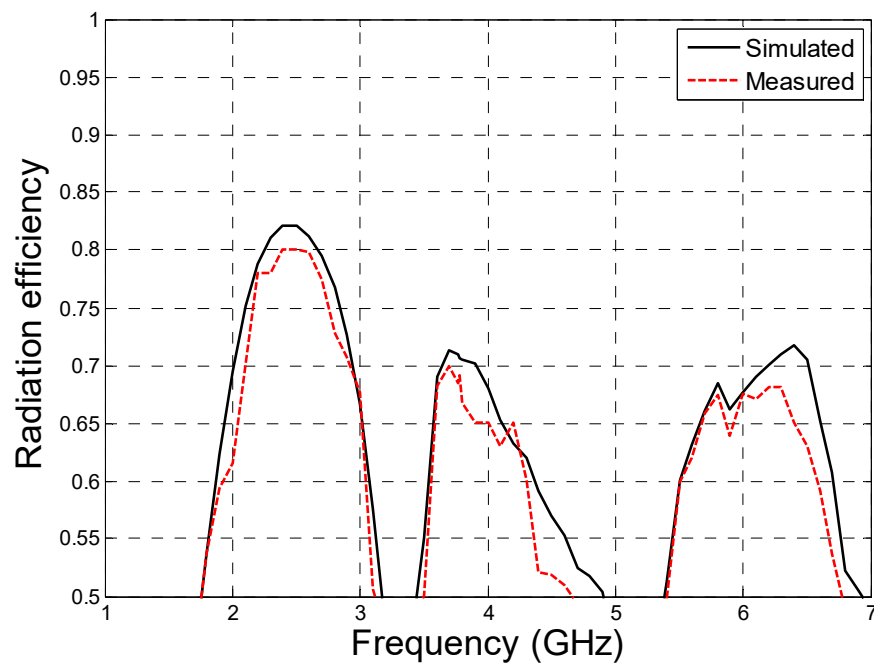


Figure 15. The radiation efficiency of the antenna as a function of frequency.

It is important to notify that the miniaturization of the antenna size should not result in deep reduction in the value of the antenna gain and bandwidth or the covering area of the radiation pattern. For example, the antenna in [29] has a very compact size ($20 \times 18 \text{ mm}^2$) with dimensions fabricated on an RT Duroid 6006 substrate with dielectric constant of 6.15 and 2.54 mm in height. The bands covered are 3.2 GHz, 4 GHz, and 5.9 GHz with fractional bandwidth of 3.12%, 2.5%, and 2.54%, respectively, and the gain was not reported. In study [30], the antenna has a compact size of ($24 \times 22 \text{ mm}^2$), but did not have an omnidirectional radiation pattern which is most appropriate for IoT application. In addition, the antenna in [31] is a UWB antenna with dimensions equal to ($15 \times 17 \text{ mm}^2$) but with

IEEE gain values less than 0 dBi for frequencies less than 5.5 GHz. On the other hand, study [32] obtains maximum gain value equal to 2 dBi with a toleration in the antenna overall dimensions of $(38 \times 25 \text{ mm}^2)$. As mentioned earlier, the proposed antenna makes a good balance between the antenna size of $(33 \times 22 \times 1.6) \text{ mm}^3$ and the antenna maximum gain values of 1.6 dBi, 0.9 dBi, and 1.1 dBi at 2.4 GHz, 3.7 GHz, and 5.8 GHz, respectively. It is worth mentioning that in spite of the reduced size of antenna, the gain value is perfect and very beneficial for IoT communication. Table 4 compares the proposed antenna structure characteristics with some other previous multiband antennas. It is clear from the table that the proposed antenna almost has a more compact size with good matching, wide bandwidth, and excellent radiation performance compared with the other configurations.

Table 4. Comparison of the proposed antenna with previous works.

Ref.	Antenna Structure	Size (mm ³)	Resonance Frequencies (GHz)	Max. Band-Width (MHz)	Gain (dBi)
[17]	Slotted	80 × 80 × 1.6	2.4, 3.5, and 5.8	140	−2.33, 3.1, and 2.89
[18]	Octahedron microstrip patch	130 × 90 × 6.15	0.85, 2.42, 3.26, 5.78	310	2.76, 3.29, 5.96, 5.5
[16]	Slotted patch	120 × 65 × 1.6	0.9, 1.1, 1.72, 2.18, 5, and 5.15	150	0.53, −0.96, 1.97, 3.75, 2.46, and 4.9
[23]	Slotted patch	48 × 48 × 1.6	1.73 and 2.53	30	−3.8 and 1.9
[19]	C-shaped	200 × 260 × 1.6	1.8, 2.4, and 5	100	2.4, 4.75, and 5.25
[25]	Slotted square	38.5 × 38.5	2.4 and 2.8	20	3.4 and 3.2
Proposed	Square split ring	33 × 22 × 1.6	2.4, 3.7, 5.8	900	1.43, 0.9, and 1.1

5. Conclusions

A new triple-band monopole antenna with split ring resonator configuration and half ring resonator is suggested and analyzed. The proposed structure is presented to obtain a compact size and low cost that makes it suitable for IoT applications. A low-cost FR4 substrate material was used for the design. The proposed antenna operates at three different bands of 2.4 GHz, 3.7 GHz, and 5.8 GHz which are very useful for IoT applications. The suggested design has several features such as small size, excellent impedance matching, simple to manufacture, and high fractional bandwidth for each band. On the other hand, the proposed antenna has an omnidirectional radiation pattern for the three bands with maximum gain values equal to 1.43 dBi, 0.9 dBi, and 1.1 dBi corresponding to each resonant frequency.

Author Contributions: Conceptualization, D.H.A.; methodology, D.H.A.; investigation, D.H.A., F.A.; resources, D.H.A., F.A., A.S.A., Y.I.A.A.-Y. and R.A.A.-A.; writing—original draft preparation, D.H.A.; writing—review and editing, D.H.A., F.A., A.S.A., Y.I.A.A.-Y. and R.A.A.-A.; visualization, D.H.A., F.A., A.S.A., Y.I.A.A.-Y. and R.A.A.-A. All authors have read and agreed to the published version of the manuscript.

Funding: This article received no external funding.

Data Availability Statement: Not applicable.

Conflicts of Interest: The authors declare no conflict of interest.

References

- Xu, K.D.; Zhang, Y.H.; Spiegel, R.J.; Fan, Y.; Joines, W.T.; Liu, Q.H. Design of a Stub-Loaded Ring-Resonator Slot for Antenna Application. *IEEE Trans. Antennas Propag.* **2015**, *63*, 517–524. [[CrossRef](#)]
- Al-Fuqaha, A.; Guizani, M.; Mohammadi, M.; Aledhari, M.; Ayyash, M. Internet of things: A survey on enabling technologies, protocols, and applications. *IEEE Commun. Surv. Tutor.* **2015**, *17*, 2347–2376. [[CrossRef](#)]
- Mao, Y.; Guo, S.; Chen, M. Compact dual-band monopole antenna with defected ground plane for Internet of things. *IET Microw. Antennas Propag.* **2018**, *12*, 1332–1338. [[CrossRef](#)]

4. Vijayvergiya, P.L.; Panigrahi, R.K. Single-layer single-patch dual band antenna for satellite applications. *IET Microw. Antennas Propag.* **2017**, *11*, 664–669. [[CrossRef](#)]
5. Liu, H.-W.; Wen, P.; Zhu, S.-S.; Ren, B.; Guan, X.; Yu, H. Quad-band CPW-fed monopole antenna based on flexible pentangle-loop radiator. *IEEE Antennas Wirel. Propag. Lett.* **2015**, *14*, 1373–1376. [[CrossRef](#)]
6. Alnahwi, F.M.; Al-Yasir, Y.I.; See, C.H.; Abd-Alhameed, R.A. Single-Element and MIMO Circularly Polarized Microstrip Antennas with Negligible Back Radiation for 5G Mid-Band Handsets. *Sensors* **2022**, *22*, 3067. [[CrossRef](#)] [[PubMed](#)]
7. Mandal, D.; Pattnaik, S.S. Quad-band wearable slot antenna with Low SAR values for 1.8 GHz DCS, 2.4 GHz WLAN and 3.6/5.5 GHz WiMAX Applications. *Prog. Electromagn. Res. B.* **2018**, *81*, 163–182. [[CrossRef](#)]
8. Du, Y.Y.; Zhao, A.P. An internal quad-band printed monopole antenna for oval-shaped mobile terminals. *IEEE Trans. Mag.* **2012**, *48*, 683–686. [[CrossRef](#)]
9. Chen, C.-C.; Sim, C.-Y.-D.; Chen, F.-S. A novel compact quad-band narrow strip-loaded printed monopole antenna. *IEEE Antennas Wirel. Propag. Lett.* **2009**, *8*, 974–976. [[CrossRef](#)]
10. Abdalla, M.A.; Hu, Z. Design and analysis of a compact quad band loaded monopole antenna with independent resonators. *Int. J. Microw. Wirel. Technol.* **2018**, *10*, 479–486. [[CrossRef](#)]
11. Cao, Y.F.; Cheung, S.W.; Yuk, T.I. A multiband slot antenna for GPS/WiMAX/WLAN systems. *IEEE Trans. Antennas Propag.* **2015**, *63*, 952–958. [[CrossRef](#)]
12. Bilotti, F.; Alu, A.; Vegni, L. Design of miniaturized metamaterial patch antennas with mu-negative loading. *IEEE Trans. Antennas Propag.* **2008**, *56*, 1640–1647. [[CrossRef](#)]
13. Ullah, M.H.; Islam, M.T.; Mandeep, J.S. A parametric study of high dielectric material substrate for small antenna design. *Int. J. Appl. Electromagn. Mech.* **2013**, *41*, 193–198. [[CrossRef](#)]
14. Alnahwi, F.; Abdalameed, A.; Swadi, H.L.; Abdullah, A.S. A compact wide-slot UWB antenna with reconfigurable and sharp dual-band notches for underlay cognitive radio applications. *Turk. J. Electr. Eng. Comput. Sci.* **2019**, *27*, 94–105. [[CrossRef](#)]
15. Yadav, N.P. Triple u-slot loaded defected ground plane antenna for multiband operations. *Microw. Opt. Technol. Lett.* **2016**, *58*, 124–128. [[CrossRef](#)]
16. Jha, K.R.; Bukhari, B.; Singh, C.; Mishra, G.; Sharma, S.K. Compact Planar Multistandard MIMO Antenna for IoT Applications. *IEEE Trans. Antennas Propag.* **2018**, *66*, 3327–3336. [[CrossRef](#)]
17. Saghati, A.P.; Azarmanesh, M.; Zaker, R.A. Novel Switchable Single- and Multifrequency Triple-Slot Antenna for 2.4-GHz Bluetooth, 3.5-GHz WiMax, and 5.8-GHz WLAN. *IEEE Antennas Wirel. Propag. Lett.* **2010**, *9*, 534–537. [[CrossRef](#)]
18. Bashir, U.; Jha, K.R.; Mishra, G.; Singh, G.; Sharma, S.K. Octahedron-Shaped Linearly Polarized Antenna for Multistandard Services Including RFID and IoT. *IEEE Trans. Antennas Propag.* **2017**, *65*, 3364–3373. [[CrossRef](#)]
19. Kulkarni, J. Multi-band printed monopole antenna conforming bandwidth requirement of GSM/WLAN/WiMAX standards. *Prog. Electromagn. Res. Lett.* **2020**, *91*, 59–66. [[CrossRef](#)]
20. Alici, K.B.; Serebryannikov, A.E.; Ozbay, E. Radiation properties and coupling analysis of a metamaterial based, dual polarization, dual band, multiple split ring resonator antenna. *J. Electromagn. Waves Appl.* **2010**, *24*, 1183–1193. [[CrossRef](#)]
21. Malik, J.; Kartikeyan, M.V. Metamaterial inspired patch antenna with L-shape slot loaded ground plane for dual band (WiMAX/WLAN) applications. *Prog. Electromagn. Res. Lett.* **2012**, *31*, 35–43. [[CrossRef](#)]
22. Si, L.M.; Lv, X. CPW-FED multi-band omni-directional planar microstrip antenna using composite metamaterial resonators for wireless communications. *Prog. Electromagn. Res. Lett.* **2008**, *83*, 133–146. [[CrossRef](#)]
23. Wang, M.; Yang, L.; Shi, Y. A Dual-port Microstrip Rectenna for Wireless Energy Harvest at LTE Band. *Int. J. Electron. Commun.* **2020**, *126*, 153451. [[CrossRef](#)]
24. Thiruvengadam, S.; Parthasarathy, E.; Palaniswamy, S.K.; Kumar, S.; Wang, L. Design and Performance Analysis of a Compact Planar MIMO Antenna for IoT Applications. *Sensors* **2021**, *21*, 7909. [[CrossRef](#)]
25. Abdulkawi, W.M.; Sheta, A.A.; Elshafiey, I.; Alkanhal, M.A. Design of Low-Profile Single- and Dual-Band Antennas for IoT Applications. *Electronics* **2021**, *10*, 2766. [[CrossRef](#)]
26. Balanis, C.A. *Antenna Theory Analysis and Design*, 4th ed.; John Wiley & Sons: Hoboken, NJ, USA, 2016.
27. CST: Computer Simulation Technology Based on FIT Method manufactured by Dassault Systèmes UK, Coventry, United Kingdom. 2018. Available online: <https://www.adaptivecorp.com/products/dassault-systemes/simulia/cst-studio-suite/> (accessed on 30 July 2022).
28. Alwareth, H.; Ibrahim, I.M.; Zakaria, Z.; Al-Gburi, A.J.A.; Ahmed, S.; Nasser, Z.A. A Wideband High-Gain Microstrip Array Antenna Integrated with Frequency-Selective Surface for Sub-6 GHz 5G Applications. *Micromachines* **2022**, *13*, 1215. [[CrossRef](#)] [[PubMed](#)]
29. David, R.M.; AW, M.S.; Ali, T.; Kumar, P. A Multiband Antenna Stacked with Novel Metamaterial SCSRR and CSSRR for WiMAX/WLAN Applications. *Micromachines* **2021**, *12*, 113. [[CrossRef](#)]
30. Naik, K.K. Asymmetric CPW-fed SRR patch antenna for WLAN/WiMAX applications. *AEU Int. J. Electron. Commun.* **2018**, *93*, 103–108. [[CrossRef](#)]

31. Al-Gburi, A.J.; Zakaria, Z.; Palandoken, M.; Ibrahim, I.M.; Althuwayb, A.A.; Ahmad, S.; Al-Bawri, S.S. Super compact uwb monopole antenna for small iot devices. *Comput. Mater. Contin.* **2022**, *73*, 2785–2799. [[CrossRef](#)]
32. Pei, J.; Wang, A.G.; Gao, S.; Leng, W. Miniaturized triple-band antenna with a defected ground plane for WLAN/WiMAX applications. *IEEE Antennas Wirel. Propag. Lett.* **2011**, *10*, 298–301.